Vol. **108** (2005) *ACTA PHYSICA POLONICA A* No. 2

Proceedings of the XXI International Meeting on Radio and Microwave Spectroscopy
RAMIS 2005, Poznań-Będlewo, Poland, April 24–28, 2005

EMR Study of Electronic and Magnetic Ordering in Doped $CaMn_{1-x,y}M_{x,y}O_3$ (M = Ru, Mo) Perovskites

A.I. Shames[a], M. Auslender[b], E. Rozenberg[a], G. Gorodetsky[a], C. Martin[c] and A. Maignan[c]

[a]Department of Physics, Ben Gurion University of the Negev
P.O. Box 653, Be'er-Sheva 84105, Israel

[b]Department of Electrical Engineering, Ben Gurion University of the Negev
P.O. Box 653, Be'er-Sheva 84105, Israel

[c]Laboratoire CRISMAT, UMR 6508, ISMRA, 14050 Caen, Cedex, France

X-band electron magnetic resonance measurements of polycrystalline $CaMn_{1-x,y}M_{x,y}O_3$ (M = Ru, $0 \leq x \leq 0.5$; M = Mo, $0 \leq y \leq 0.14$) samples were performed at 120 K $\leq T \leq$ 540 K. The observed anomalies of electron magnetic resonance parameters correlate pretty well with the temperatures of antiferro-, ferromagnetic-like, and orbital/charge-ordering transitions in these systems and specify phase diagrams obtained by other techniques. However, a strong difference between resonant properties of Ru- and Mo-doped series is observed in both paramagnetic and magnetically ordered states. To describe such a difference, the energy bands diagrams, which comprise the deep impurity t_{2g}-like states + e_g-like conductive band for $CaMn_{1-x}Ru_xO_3$ and shallow impurity states + conductive band, both having e_g-like symmetry, for $CaMn_{1-y}Mo_yO_3$, are proposed. Specific electrons' contribution to the electron magnetic resonance line width explains concentration and temperature dependences of this parameter in the paramagnetic state in considered systems.

PACS numbers: 75.30.Kz, 75.47.Lx, 76.30.–v, 76.50.+g

1. Introduction

It is well established now [1–6] that electrons may be introduced into the G-type antiferromagnetic (AFM) insulator $CaMnO_3$ with the Néel temperature

$T_N \approx 120$ K by respective substitution of Ca or Mn sites with a trivalent lanthanide [1, 2] or with a metal having a valency larger than 4+ [3–6]. Such a doping causes formation of Mn^{3+} species for preserving the charge balance in a system and an appearance of electrons, hopping between Mn^{4+} and Mn^{3+} ions. For example, substitution of Mn by Ru leads to development of ferromagnetism (FM), which appears as the long-range ordered phase within AFM matrix of $CaMn_{1-x}Ru_xO_3$ (CMRO) system for Ru-doping $x \geq 0.10$ [3]. The metal-like conductivity due to FM double exchange mechanism becomes prevailing when FM clusters percolate for $x \geq 0.20$. As a result, the inhomogeneous ground state, comprising FM metallic- and AFM insulating-like regions, appears in CMRO [3]. In a marked contrast, doping of $CaMnO_3$ with Mo induces FM-like state and enhances metallicity just for low Mo concentrations $y \leq 0.06$, while further substitution of Mn-sites with Mo leads to suppression of FM interactions which causes C-type AFM state, observed in $CaMn_{1-y}Mo_yO_3$ (CMMO) system for $y > 0.06$ [5, 6]. Moreover, the orbital/charge ordering (OO/CO) develops in the interval $T_{OO} < T < T_N$ for $0.06 < y < 0.12$ and within $0 < T < T_{OO}$ for $y > 0.12$ [6]. Let us note that CMRO has an orthorhombic P*nma* structure independently of x value, while monoclinic $P2_1/m$ distortions are observed in CMMO below the transition temperature T_{OO} for $y > 0.06$ [5, 6]. It is evident that, for obtaining a deeper insight into the magnetic ordering in these systems and for better understanding of underlying physics, microscopic probes, capable to identify signatures of different exchange interactions, are required. For example, our measurements [7, 8] of electron magnetic resonance (EMR, comprising both electron paramagnetic resonance — EPR — for $T > T_C$, the Curie point, and ferromagnetic resonance — FMR — for $T < T_C$) in CMRO with $x \leq 0.40$ show that EMR parameters differ drastically for AFM and AFM+FM samples with respective Ru-doping $x \leq 0.06$ and $x \geq 0.10$.

2. Experimental

The main goal of this comparative study is EMR probing of changes in the magnetic structure of $CaMn_{1-x,y}M_{x,y}O_3$ system during Ru- and Mo-doping of the Mn-sites. The synthesis of polycrystalline samples of CMRO and CMMO with $0 \leq x \leq 0.50$ and $0 \leq y \leq 0.14$, respectively, has been described previously (see [4–8] and refs. therein). The room temperature (RT) X-ray diffraction, electron diffraction, and energy dispersive spectroscopy in the range 92 K $< T <$ 300 K were explored for checking the single-phase nature, purity, and homogeneity of cationic compositions of the samples studied. The EMR spectra of all CMRO and CMMO samples were recorded using Bruker EMX-220 X-band ($\nu = 9.4$ GHz) spectrometer in the range of $120(\pm 0.5)$ K $\leq T \leq 540(\pm 0.5)$ K. The measurements were carried out using loose-packed micron-sized ($5-20$ μm) crushed samples. The details regarding the measurement technique and the reasons for using loose-packed samples may be found in Ref. [9]. Temperature dependences of the resonance field

H_r, line width ΔH_{pp}, double integrated intensity DIN (which is proportional to the EMR susceptibility χ_{EMR}) and the line shape were analyzed. DIN values were obtained taking into account bias and slope corrections in the case of $\Delta H_{pp} \geq H_r$.

3. Results and discussion

At RT the pristine $CaMnO_3$ compound shows Lorentzian-like line ($\Delta H_{pp} =$ 170 mT) centered at $g = 1.98 \pm 0.01$. Progressive Ru-doping practically does not affect the position of the corresponding EMR lines, but leads to a significant line broadening. For $x \geq 0.06$ the line width exceeds the spectrometer sweep range of 1 T, for instance up to $\Delta H_{pp} = 1.33$ T for $x = 0.15$ (see Fig. 1). At higher Ru-doping levels the line width is practically indefinable. This effect is less pronounced for CMMO system, e.g., a comparable doping level of $y = 0.14$ broadens EMR line up to 300 mT (Fig. 1). The quasi-linear character of such an increase is observed for both Ru and Mo dopants.

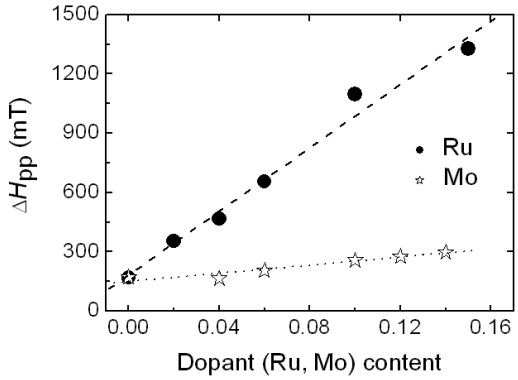

Fig. 1. The EMR line width ΔH_{pp} dependences versus concentrations of Ru- and Mo-dopants at $T = 300$ K.

Results of the temperature dependent EMR study may be divided into two groups containing data for low and high dopants' concentrations: $0 \leq x \leq 0.06$, $0 \leq y \leq 0.06$ and $0.10 \leq x \leq 0.50$, $0.10 \leq y \leq 0.14$, respectively. At lowest temperatures no EMR signals were observed for the CMRO samples with $x = 0$, 0.02, 0.04, and 0.06. The spectrum of the pristine sample at $T = T_N = 120$ K (not shown here) represents solely the background signal. In contrast, low doped ($y = 0.04$ and 0.06) CMMO samples demonstrate strong signals just within the low temperature range (Fig. 2b, bottom). The EMR spectra for $x > 0.06$ CMRO samples are plotted in the top of Fig. 2a. The notable shift of H_r toward lower fields and appearance of additional resonance lines for the highest doping levels are clearly seen. These facts give an unambiguous EMR evidence of FM ordering [9]. On the other hand, highly-doped CMMO samples ($y \geq 0.10$) show inverse

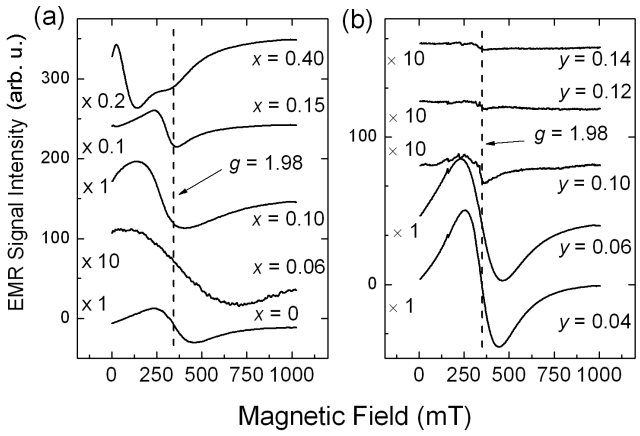

Fig. 2. EMR spectra of: (a) CMRO as a function of x, $T = 140$ K, $\nu = 9.438$ GHz; and (b) CMMO as a function of y, $T = 160$ K, $\nu = 9.434$ GHz. For each series the spectra were normalized to the unit mass, plotted using multiplication constants drawn on the left side of each part and vertically shifted for clarity. Vertical dashed lines mark $g = 1.98$ position.

behavior of EMR lines which drop down and disappear at temperature decreasing (Fig. 2b, top).

The temperature dependences of DIN in Figs. 3a and b manifest the clear difference between the low- ($x,\ y \leq 0.06$) and highly-doped ($x,\ y \geq 0.10$) samples. Comparably doped by Ru and Mo series reveal: (i) the opposite temperature trends i.e., respective decrease and increase in DIN values upon cooling for compounds, low-doped with Ru and Mo ($x,\ y \leq 0.06$), see Fig. 3a; and (ii) the sharp peaks of DIN near the critical temperatures of magnetic transitions, which demonstrate CMRO specimens with $x \geq 0.10$. These peaks exceed the DIN maxima observed for the CMMO ($y \geq 0.10$) samples by an order of magnitude, see Fig. 3b.

Figures 3c and d shows that $\Delta H_{\rm pp}$ of low-doped CMRO increases upon cooling, whereas line widths od highly-doped CMRO decrease with the decrease in temperature passing through characteristic minima and then increase again. Line widths of all CMMO samples increase upon cooling. Such an increase is relatively weak and gradual down to some characteristic temperature $T^* = T^*(y)$, e.g., $T^* \approx 150$ K and 340 K for $y = 0.04$ and 0.14. However, it becomes much stronger at $T \leq T^*$ for both low- ($y \leq 0.06$) and high-doped ($y \geq 0.10$) samples. Let us note that the line-width broadening at $T < T^*$ for $y \geq 0.10$ compounds is markedly enhanced comparing to this one for $y \leq 0.06$ samples.

Let us discuss briefly the results obtained, addressing mainly how the electronic structures, established by Ru- and Mo-doping of Mn-sites, affect EMR characteristics. These structures are revisited in view of a marked difference between

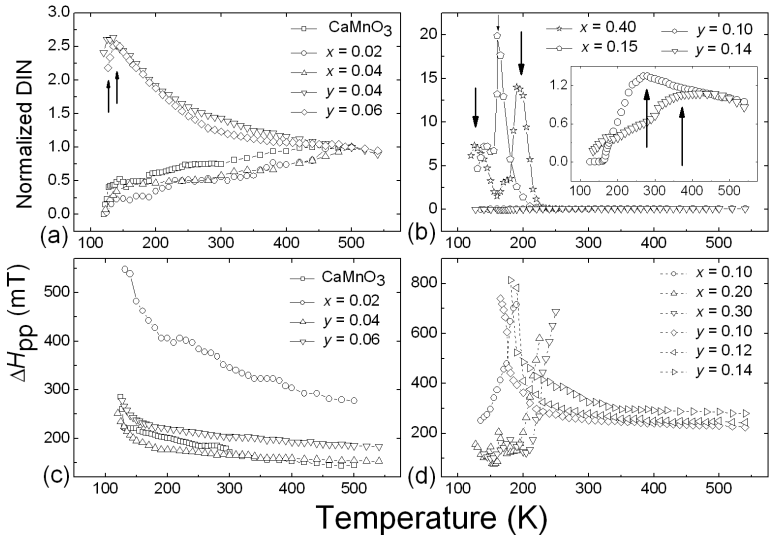

Fig. 3. Temperature dependences of EMR spectra parameters. Normalized double integrated intensity of EMR signals (DIN): (a) pristine $CaMnO_3$, low-doped CMRO and CMMO samples; (b) highly-doped samples CMRO and CMMO, inset — zoom of $y = 0.10$ and 0.14 samples. Arrows in (a) and (b) mark the DIN vs. T maxima. Line width $\Delta H_{\rm pp}$: (c) low-doped CMRO and CMMO samples, (d) highly doped CMRO and CMMO samples.

the EMR properties of CMRO and CMMO (see Figs. 1–3). The following valence formulae [4, 5] are accepted by us: $Ca(Mn^{4+})_{1-2x}(Mn^{3+})_x(Ru^{5+})_xO_3$ and $Ca(Mn^{4+})_{1-3y}(Mn^{3+})_{2y}(Mo^{6+})_yO_3$. Thus, Ru-doping decreases Mn^{4+} content to $1-2x$, and increases the Mn^{3+} one to x per formula unit. Let us assume that extra (to core Ru^{5+} ions) d electrons are either trapped at bound state near Ru^{5+} or hop via empty $3d$ $e_{\rm g}$ states of host Mn^{4+}, i.e. perform band motion. Thus, no Mn^{3+} ions, in the strict sense, appear since the valence state of x Mn ions fluctuates between 4+ and 3+ with some characteristic electron-hopping frequency. The absence of stable Jahn–Teller (JT) Mn^{3+} ions in CMRO is strongly supported by the absence of OO/CO states for x up to 0.50 [4, 8]. It advocates the energy diagram, in which the deep trap level, with symmetry other than $e_{\rm g}$, appears below the conduction band with Ru-doping (Fig. 4a, top). We suggest that there is high admixture of $4d$ $t_{2\rm g}$ states in this bound state. Thus, "Ru^{5+} + bound-electron" complex may be much mimicked by Ru^{4+}. At higher x this deep trap level turns to separated impurity band (Fig. 4a, bottom). Concerning the Mo-doping, the above noted valence formula means that two d electrons leave Mo^{4+} for sitting in, or jumping over the Mn^{4+} $3d$ $e_{\rm g}$ states. Let us note that, due to the highly effective charge of the Mo^{6+} defect, a partial trapping of electrons nearby the defect cannot be excluded. We speculate that this possible impurity state is $e_{\rm g}$-like

since the electrons are to hop far enough from Mo^{6+}, which forms a high potential barrier. This level is shallower than t_{2g}-like one for Ru^{5+}; hence, the exchange interaction with Mn^{4+} ions is stronger for the electron on the former level than on the latter one. The energy diagram, which we suggest for CMMO, consists of the conduction and shallow impurity bands at small y (Fig. 4b, top) and a merged conduction band at higher y (Fig. 4b, bottom). Such merging leads to the onset of OO states at $y \geq 0.06$ in CMMO. As a whole, these energy diagrams (Fig. 4) are consistent with the magnetic and conductive properties of Ru- and Mo-doped $CaMnO_3$ [4–8], but the detailed consideration with this respect will be presented elsewhere.

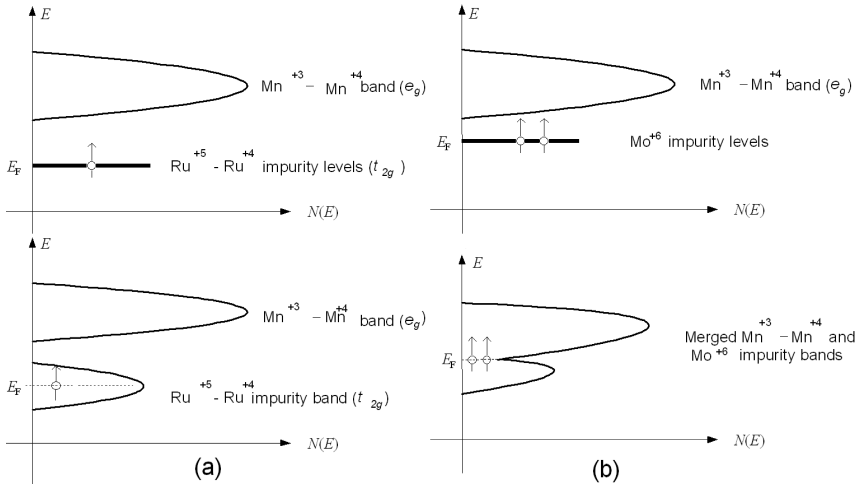

Fig. 4. Energy diagrams for: (a) CMRO, comprising deep impurity t_{2g}-like states (band) + e_g conduction band; and (b) CMMO, comprising shallow impurity e_g-like states (band) + e_g conduction band.

Let us outline the spin subsystems in CMRO and CMMO, which play the main role in EMR in these systems. Common to both are: (i) Mn^{4+} ions and (ii) ensembles of conduction electrons spins. In contrast, the (iii) bound-electrons spins subsystems (iii) are quite different in these systems. Namely, (ii) and (iii) may be considered as having the same e_g symmetry in CMMO, while the symmetry of the bound-state wave function is supposedly t_{2g}-like in CMRO. In addition, there are two specific subsystems: (iv) the Ru^{5+} spins in CMRO and (v) the Mn^{3+} spins in CMMO with $y > 0.06$. The (v) subsystem emerges at $T_N < T < T_{OO}$, when all the doped electrons become captured in Mn^{3+} as a result of the JT effect. These subsystems are exchange-coupled to each other. Hence, the reasonable concept is the "bottleneck" one, i.e. the only relevant for the EMR variable is the total — over all subsystems — spin. Then, see e.g. Ref. [10], one obtains for the EMR line width

$$\gamma_{\text{eff}}\Delta H_{\text{pp}} = \frac{L}{k_{\text{B}}T\chi}, \tag{1}$$

here χ is the total spin susceptibility and L is so-called Onsager coefficient, whose physical meaning is a nominal total spin relaxation frequency. Assuming that our spin subsystems do not interfere, when relaxing, one obtains $\Delta H_{\text{pp}} = \Delta H_{\text{pp,i}} + \Delta H_{\text{pp,e}}$, which are sums of partial line widths over different ions and electrons species, respectively. The dependence of $\Delta H_{\text{pp,i}}$ on T; $c = x,\ y$ etc. may be revealed using the Curie–Weiss approximation for χ, giving

$$\Delta H_{\text{pp,i,e}}(T,c) = \frac{T - \Theta_{\text{CW}}}{T}\frac{L_{\text{i,e}}(T,c)}{C\gamma_{\text{eff}}}, \tag{2}$$

where Θ_{CW} is the Curie–Weiss temperature and C the Curie constant, both being doping-controlled parameters. The T- and c-trends of $L_{\text{e}}(T,c)$ may be guessed using the proposed energy diagrams and knowledge about spin relaxation of charge carriers in non-correlated conductors [11]. It is obvious that $L_{\text{e}}(T,c)$ should increase with increasing doping level c: the more electrons the stronger the relaxation channel. The scale of $L_{\text{e}}(T,c)$ is determined by electron spin-reversing transitions (SRTs) appearing due to spin-orbital interactions (SOIs). One type of SRT stems from mixing of spin-up and spin-down states by periodic crystal potential SOI, while the other one happens between such unperturbed states by direct SOI on the impurity and deformation potentials. For the states with nonzero or slightly frozen orbital moment, e.g., those of (iii) in CMRO, the first SRT dominates $L_{\text{e}}(T,c)$. For the states of subsystem (ii) with the frozen orbital moment, the second SRT dominates $L_{\text{e}}(T,c)$. Thus, whatever x and y, $L_{\text{e}}(T,y)$ for CMMO (in which most electrons are in the e_{g}-like conduction band) must be much smaller than $L_{\text{e}}(T,x)$ for CMRO, in which most electrons are in the $t_{2\text{g}}$-like impurity states. Thus, Eq. (2) satisfactorily describes concentration dependences of ΔH_{pp} in Fig. 1. Above noted inequality $L_{\text{e}}(T,x) > L_{\text{e}}(T,y)$ may account for striking difference between the line widths in CMMO and CMRO. The sharp decrease in ΔH_{pp} in highly-doped ($x \geq 0.06$) CMRO upon cooling (Fig. 3d) may be explained due to phonons' "freezing", reducing orbital–lattice relaxation. Above noted mostly pronounced low temperature broadening of ΔH_{pp} in CMRO ($x \leq 0.06$) and CMMO ($y \leq 0.10$), shown in Figs. 3c and d, coincides with the transition to AFM state upon cooling at $T < T_{\text{N}} \approx 125$ K [4, 8] and at $T < T_{\text{N}} \approx 150$ K [5, 6] in CMRO and CMMO, respectively. Such broadening correlates also with the notable reduction of the corresponding DIN values at low T in both CMRO and CMMO (see Fig. 3 and inset in Fig. 3b).

Pronounced maxima on DIN vs. T dependences, observed in CMMO for $y \geq 0.10$ in the vicinity of OO–CO transition [6], see inset in Fig. 3b, may be explained following Bao et al. [12]. That is to say, the CO order parameter in CMMO system grows below $T_{\text{OO-CO}}$ and FM spin fluctuations are gradually replaced by AFM ones up to T_{N}, below which a perfect CO AFM state exists. This process results in decrease in DIN values below its maxima and enhancement

of $\Delta H_{\rm pp}$ broadening vs. T at $T < T^*$ (see inset in Fig. 3b and Fig. 3d). Below $T_{\rm N}$ the AFM gap in the energy spectrum of the considered compounds is opened and EMR signals become unobservable at frequencies $\nu \approx 10$ GHz. Finally, let us note that electrons introduced in $CaMnO_3$ by low Mo-doping induce FM interactions, instead of being captured (as it occurs for higher Mo contents) [4–6]. This FM-like state manifests itself in pronounced increase in DIN and its sharp maxima upon cooling for low Mo-doped compounds in a clear contrast to decrease in DIN in AFM low Ru-doped ones (see Fig. 3a).

Acknowledgments

This work was supported by the ISF grant 209/01.

References

[1] C.D. Ling, E. Granado, J.J. Neumeier, J.W. Lynn, D.N. Argyriou, *Phys. Rev. B* **68**, 134439 (2003).

[2] M. Respaud, J.M. Broto, H. Rakomo, J. Vanacken, P. Wagner, C. Martin, A. Maignan, B. Raveau, *Phys. Rev. B* **63**, 144426 (2001).

[3] A. Maignan, C. Martin, M. Hervieu, B. Raveau, *Solid State Commun.* **117**, 377 (2001).

[4] L. Pi, S. Hebert, C. Martin, A. Maignan, B. Raveau, *Phys. Rev. B* **67**, 024430 (2003).

[5] C. Martin, A. Maignan, M. Hervieu, B. Raveau, J. Hejtmanek, *Phys. Rev. B* **63**, 100406 (2001).

[6] A. Maignan, C. Martin, C. Autret, M. Hervieu, B. Raveau, J. Hejtmanek, *J. Mater. Chem.* **12**, 1806 (2002).

[7] A.I. Shames, E. Rozenberg, G. Gorodetsky, A. Maignan, C. Martin, M. Hervieu, B. Raveau, *J. Magn. Magn. Mater.* **272-276**, Suppl., e1627 (2004).

[8] A.I. Shames, E. Rozenberg, C. Martin, A. Maignan, B. Raveau, G. Andre, G. Gorodetsky, *Phys. Rev. B* **70**, 134433 (2004).

[9] A.I. Shames, E. Rozenberg, V. Markovich, M. Auslender, A. Yakubovsky, A. Maignan, C. Martin, B. Raveau, G. Gorodetsky, *Solid State Commun.* **126**, 395 (2003).

[10] D.L. Huber, G. Alejandro, A. Caneiro, M.T. Causa, F. Prado, M. Tovar, S.B. Oseroff, *Phys. Rev. B* **60**, 12155 (1999).

[11] V.F. Gantmakher, Y.B. Levinson, *Carrier Scattering in Metals and Semiconductors*, North-Holland, Amsterdam 1987.

[12] Wei Bao, J.D. Axe, C.H. Chen, S-W. Cheong, *Phys. Rev. Lett.* **78**, 543 (1997).